Talanta 84 (2011) 374–381

Contents lists available at ScienceDirect

Talanta

journal homepage: www.elsevier.com/locate/talanta

Simultaneous determination of soluble manganese(III), manganese(II) and total manganese in natural (pore)waters

Andrew S. Madison[a,*], Bradley M. Tebo[b], George W. Luther III[a,*]

[a] School of Marine Science and Policy, College of Earth, Ocean and Environment, University of Delaware, Lewes, DE 19958, USA
[b] Division of Environmental and Biomolecular Systems, OGI School of Science and Engineering, Oregon Health and Science University, Beaverton, OR 97006, USA

ARTICLE INFO

Article history:
Received 22 November 2010
Received in revised form 4 January 2011
Accepted 11 January 2011
Available online 19 January 2011

Keywords:
Manganese
St. Lawrence
Complexation
Sediment
Natural organic-ligands
Spectrophotometric method

ABSTRACT

A new spectrophotometric protocol was developed for the simultaneous determination of soluble Mn(III), Mn(II) and total Mn [sum of soluble Mn(III) and Mn(II)] in sediment porewaters using a water soluble meso-substituted porphyrin [α,β,γ,δ-tetrakis(4-carboxyphenyl)porphine (T(4-CP)P)]. A simple kinetic rate model is used to quantify soluble Mn(II), Mn(III) and total Mn concentrations during a metal substitution reaction. Under optimized conditions, the method accurately determines soluble Mn(II) and Mn(III) within a concentration range of 100 nM–10 μM. The detection limit of total soluble Mn is 50 nM. Using this method, soluble Mn(II) and Mn(III) concentrations were determined in standard solutions within 0.4–2% of the known values and agreed closely with results of inductively coupled plasma mass spectrometric and voltammetric analyses. The procedure was successfully applied to determine soluble Mn(II), Mn(III) and total Mn in sediment porewaters of the Lower St. Lawrence Estuary. Mn(III) represented up to 85% of the total soluble Mn pool in surface sediments.

1. Introduction

Manganese plays an important role in geochemical cycles in sediments and the water column, in addition to being a fundamental trace nutrient for essentially all organisms. Traditionally, manganese (Mn) speciation has been defined by filtration. Any Mn that passes through 0.2 or 0.45 μm filters is defined as the soluble Mn fraction, which is assumed to be Mn(II), while the particulate fraction that is retained is Mn(III,IV) oxides. Although soluble Mn(III) persists as complexes in laboratory solutions, its occurrence in natural waters is largely ignored because as an uncomplexed, free ion, any inorganic Mn(III) formed would rapidly disproportionate to Mn(II) and MnO_2 [1]. As a result, the focus of most Mn speciation studies has been on the distribution and reactivity of the soluble free ion Mn(II) and particulate Mn(III,IV) oxides [2–6]. However, soluble Mn(III) can be detected in aquatic environments when it is stabilized in the presence of strong organic or inorganic ligands, such as desferrioxamine B [7], pyrophosphate [8], citrate [1], and a pyoverdine ligand [9]. Recent work by Trouwborst et al. [10] and Yakushev et al. [11,12] document the existence of soluble Mn(III) forms in natural waters, which account for up to 100% of the dissolved Mn pool in the suboxic zones of the Black Sea and Baltic Sea.

To our knowledge, soluble Mn(III) has never been measured in sediment porewaters, most likely because a direct method capable of retaining accuracy in a variety of sedimentary environments does not exist. Hence, accurate measurements of soluble Mn(III) in sediment porewaters at the levels expected in many environments require a new approach that meets the following requirements: (1) selectivity towards both soluble Mn(II) and Mn(III), (2) accurate determination of soluble Mn(II) and Mn(III), (3) low cost of instrumentation and (4) detection limit below 1 μM when a small volume (100 μl) of sample is available.

In this contribution we present a novel approach for the rapid and simultaneous determination of soluble Mn(II) and Mn(III) in sediment porewaters via significant modification of the procedure developed by Ishii et al. [13]. This method employs a water soluble meso-substituted porphyrin [α,β,γ,δ-tetrakis(4-carboxyphenyl)porphine], which is a highly sensitive chromogenic reagent for Mn detection at nM to μM levels ($\varepsilon_{468\,nm} = 95{,}400\,M^{-1}cm^{-1}$). Soluble Mn(II) and Mn(III) are quantified with a simple kinetic rate model during a metal substitution reaction with a cadmium(II)–T(4-CP)P complex. This method was used to determine soluble Mn(II), Mn(III) and total Mn [sum of soluble Mn(II) and soluble Mn(III)] concentrations in sediment porewaters extracted from a core recovered in the Lower St. Lawrence Estuary in 2009.

* Corresponding authors at: School of Marine Science and Policy, College of Earth, Ocean and Environment, University of Delaware, 700 Pilottown Road, Lewes, DE 19958, USA. Tel.: +1 302 645 4208; fax: +1 302 645 4007.
E-mail addresses: amadison@udel.edu (A.S. Madison), tebo@ebs.ogi.edu (B.M. Tebo), luther@udel.edu (G.W. Luther III).

0039-9140/$ – see front matter © 2011 Elsevier B.V. All rights reserved.
doi:10.1016/j.talanta.2011.01.025

2. Experimental

2.1. Chemicals and materials

All chemicals were A.C.S. reagent grade. All solutions were prepared with deionized water (18.3 MΩ). A 2×10^{-4} M α,β,γ,δ-tetrakis(4-carboxyphenyl)porphine [T(4-CP)P] solution was prepared by dissolving 79.1 mg of T(4-CP)P in 5 mL of 0.1 M sodium hydroxide and diluting to 500 mL with water. This solution was stored in a polypropylene bottle, which was wrapped in aluminum foil to block ambient light. T(4-CP)P was prepared from a propionic acid solution of 4-carboxybenzaldehyde (0.24 M) and pyrrole (0.24 M) under reflux for 4 h [13,14]. (A 4 h reflux time was determined to yield a two-fold increase in product, compared to the recommended 6 h reflux time.) After cooling, the purple crystals of T(4-CP)P were recrystallized in warm methanol, filtered and cooled. A small amount of chloroform was added to initiate crystallization. A 2×10^{-4} M T(4-CP)P solution was analyzed by mass spectrometry and the T(4-CP)P purity was determined to be greater than 99% pure.

A buffer solution was prepared by adding: 50 mL of 0.025 M sodium tetraborate, 20 mL of 0.1 M hydrochloric acid (HCl) and 25 mL of 0.6 M imidazole. The pH was adjusted to 8.0 with 3 M HCl and diluted to 100 mL in a volumetric flask. A 1.2 mM cadmium chloride solution was prepared by dissolving 0.022 g of $CdCl_2$ in 100 mL of deionized water. All Mn(II) standard solutions were prepared from $MnCl_2{\cdot}6H_2O$ salt.

Two soluble Mn(III) solutions were prepared, a Mn(III)-pyrophosphate solution (Mn(III)-PP) and a Mn(III)-desferrioxamine B solution (Mn(III)-DFOB). A 5 mM pyrophosphate solution was prepared by adding 0.223 g of sodium pyrophosphate ($Na_4P_2O_7{\cdot}10H_2O$) to 100 mL of de-oxygenated deionized water and adjusting the pH to 7.0 with 3 M HCl. Once the pyrophosphate dissolved, 0.0244 g of Mn(III)-acetate salt was added to give a clear pink solution of approximately 1 mM Mn(III)-PP. The concentration of Mn(III) was determined using its absorbance peak at 484 nm and/or via an iodometric titration [10]. Typical yields of this method are greater than 98% of the total Mn(III)-acetate added. A Mn(III)-DFOB solution was prepared by dissolving 0.0657 g of desferrioxamine B mesylate salt in 100 mL of deionized water and adjusting the pH to 9.0. Then, 0.0117 g of $MnCl_2{\cdot}6H_2O$ was added and air was bubbled through the solution to stimulate the oxidation of Mn(II) to Mn(III), which is catalyzed by DFOB [7]. The solution was aerated overnight to allow maximum Mn(II) oxidation. After approximately 12 h, the pH was adjusted to 8.0 and the concentration of Mn(III)-DFOB was determined using its absorbance peak at 310 nm and/or via an iodometric titration. Mn(III) yields were typically around 85%.

Two other solutions were prepared to test for possible interferences. First, a 500 μM Mn(II)-DFOB solution was prepared by mixing 5 mL of 1 mM Mn(II) solution with 5 mL of 1 mM DFOB solution prepared in 0.025 M borate buffer (pH 7.8). The solution was allowed to equilibrate (in air) for 20 min to ensure complete Mn(II) complexation. Over the course of experimentation, up to 1-h after initial mixing, no measureable amount of Mn(III)-DFOB formed, which would interfere with the kinetic experiments (discussion below in Section 3.1). Second, a colloidal form of soluble manganese dioxide (MnO_2) was prepared according to Perez-Benitez et al. [15] by exact titration of permanganate with thiosulfate to produce colloidal MnO_2, free of Mn(II).

2.2. Absorbance measurements

A Hewlett Packard 8452B diode array spectrophotometer controlled with Olis, Inc. Globalworks software was used for all UV/vis measurements (2 nm wavelength resolution). The Mn(III)–T(4-CP)P complex was measured at its absorbance maximum (468 nm) against a reagent blank in a 1 cm pathlength quartz cell.

2.3. Procedure

An initial reagent blank is prepared in a 1 cm pathlength quartz cell (3 mL total volume) by successively adding 360 μL of T(4-CP)P (24 μM), 120 μL of borate buffer mix and 60 μL of $CdCl_2$ (24 μM). Deionized water is added to fill to total volume and the absorbance blank is measured at 468 nm. To start the kinetic experiment, the appropriate amount (100 μL) of standard or sample is added to the cell so that the sample is diluted in the reagents to yield a total Mn concentration in the range of 50 nM–10 μM. The absorbance is recorded at time zero (Mn addition) and the increase in absorbance of the Mn(III)–T(4-CP)P peak at 468 nm is monitored for approximately 15 min. To date, all laboratory and field samples reach the absorbance maximum within 15 min, except for Mn(III)-DFOB, which has a high thermodynamic stability of $\log K = 29.9$ (see below; Section 3.1) [7]. Because the accuracy of the kinetic model is dependent on the number of measurements taken, a sampling frequency of one measurement per 5 s was determined to provide accurate results.

2.4. Determination of Mn(II) and Mn(III) in the Lower St. Lawrence Estuary sediment porewaters

An undisturbed sediment core was recovered from Station 23 (48° 42.08′N/68° 39.0′W) in the hypoxic zone of the Laurentian Trough using a 0.12 m^2 Ocean Instruments Mark II box corer. The 40 cm+ long core was immediately sectioned at various depth intervals in a N_2 purged glove box to prevent oxidation of anoxic sediment [16]. Approximately 50 mL of porewater was extracted from each depth interval using Reeburgh-type squeezers [17], modified to filter the water through a 0.45 μm Type HA Millipore® filter as it passed directly into a 50 cc pre-cleaned syringe. The porewaters for Mn determination were sub-sampled from the syringes under a steady stream of Ar in a glove bag. The sub-samples were immediately analyzed with the T(4-CP)P kinetic method to determine soluble Mn(II) and Mn(III) concentrations. Because of high Mn concentrations, small volumes (100 μL) of sample were typically used for analysis. In addition to diluting the Mn within a range of 1–10 μM, the dilution also reduced chloride interference due to Cd–chloride complexation. Samples were analyzed in duplicate. To check the accuracy of the kinetic model, a Mn(II) standard (generally 2 μM) was added to each porewater sample and analyzed in duplicate. Thus, each sample was measured in quadruplicate. The Mn(II) concentration increase determined by the kinetic model always agreed within 2% of the standard addition. In addition, the rate of Mn(III)–T(4-CP)P complex formation (k_1) determined for the Mn(II) addition and oxidation in the standards was nearly identical to the Mn(II) complex formation rate in the porewater samples.

3. Results and discussion

3.1. Porphyrin method

The Mn determination method was modeled after Ishii et al. [13] because T(4-CP)P forms a Mn complex that is more sensitive than traditional methods, such as the formaldoxime method [18], and without interference from other chemical species such as iron [14]. Furthermore, quantification of total soluble Mn by the T(4-CP)P method agrees more closely with determinations via atomic absorbance spectrometry and inductively coupled plasma mass spectrometry (ICP-MS) than the formaldoxime method [14]. As shown in Fig. 1A, the Soret band of Mn(III)–T(4-CP)P at 468 nm

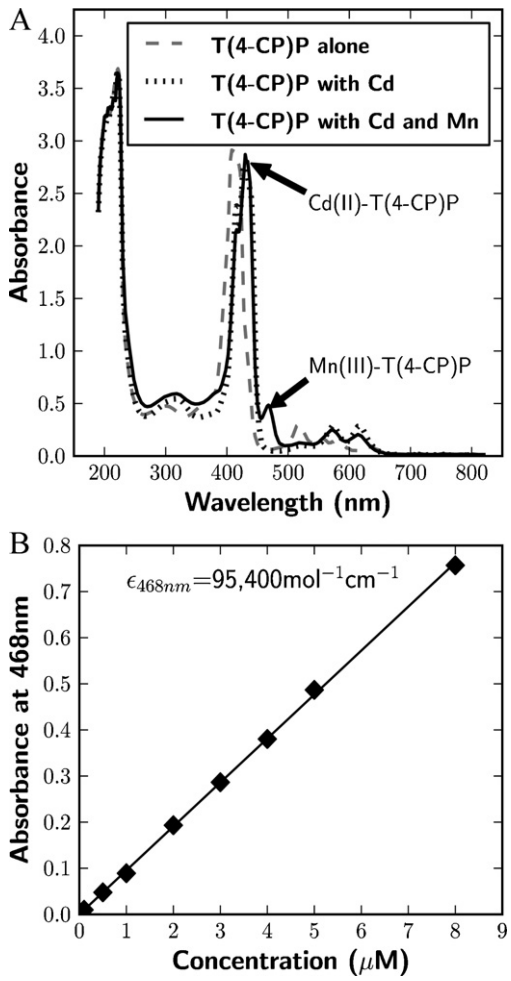

Fig. 1. (A) UV/vis spectra of T(4-CP)P, Cd(II)–T(4-CP)P and Mn(III)–T(4-CP)P. The Mn(III)–T(4-CP)P peak is located at 468 nm and the Cd(II)–T(4-CP)P peak located at 433 nm. (B) Plot of absorbance against Mn(III)–T(4-CP)P concentration.

is resolved from the peaks of T(4-CP)P (415 nm) and Cd(II)–T(4-CP)P (432 nm). The molar absorptivity of Mn(III)–T(4-CP)P was determined to be 95,400 M^{-1} cm^{-1} (Fig. 1B), in agreement with Ishii et al. [13]. The detection limit of total soluble Mn was determined via standard analytical methods (absorbance of blank plus three times its standard deviation) [19] and is estimated at 50 nM.

Ishii et al. [13] determined that Mn(II) complexation by T(4-CP)P occurs via a metal substitution reaction with Cd(II). When Mn(II) is added to a solution containing the Cd(II)–T(4-CP)P complex, the higher stability of the Mn–T(4-CP)P complex, at a pH of 7.5–8, results in an exchange of Cd(II) for Mn(II). The addition of imidazole catalyzes this substitution, which is complete in approximately 1 min. Ishii et al. [13] proposed a mechanism that once Mn(II) exchanges for the Cd^{2+} center in Cd(II)–T(4-CP)P to form Mn(II)–T(4-CP)P, the Mn(II) center is immediately oxidized by dissolved oxygen to form Mn(III)–T(4-CP)P. The Mn(III) has a d^4 electron configuration, which makes Mn(III)–T(4-CP)P further stable to oxidation and reduction because of Jahn-Teller stabilization, as seen in other Mn(III) porphyrin complexes [20].

Ishii et al. [13] and Chiswell and O'Halloran [14] examined only the kinetics of dissolved Mn(II) complexation with T(4-CP)P, ignoring possible binding with soluble Mn(III) species. Nevertheless, soluble Mn(III) reacts with the stable Cd(II)–T(4-CP)P complex via a simple exchange with Cd(II). Therefore, both Mn(II) and Mn(III) can

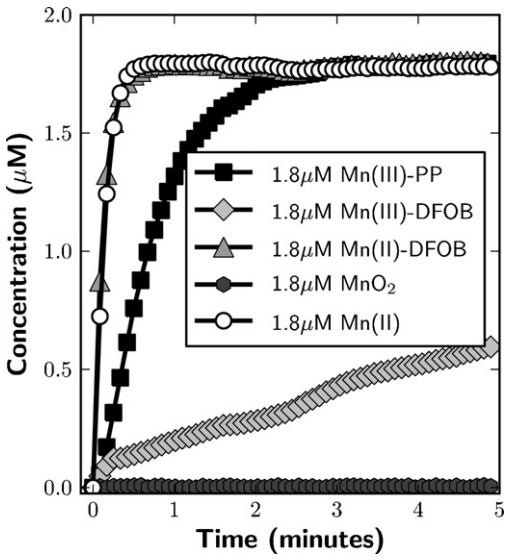

Fig. 2. Comparison of the Mn(III)–T(4-CP)P complex formation rate for Mn(III)-PP, Mn(III)-DFOB, Mn(II)-DFOB, MnO_2 and Mn(II).

react with T(4-CP)P to form the same end product Mn(III)–T(4-CP)P via separate reaction pathways, as shown in Eqs. (1) and (2).

$$\mathrm{Mn(II) + Cd\text{–}T(4\text{-}CP)P \xrightarrow{\uparrow Cd(II)} Mn(II)\text{–}T(4\text{-}CP)P + O_2} \rightarrow \mathrm{Mn(III)\text{–}T(4\text{-}CP)P} \quad (1)$$

$$\mathrm{Mn(III) + Cd\text{–}T(4\text{-}CP)P \xrightarrow{\uparrow Cd(II)} Mn(III)\text{–}T(4\text{-}CP)P} \quad (2)$$

Because Mn(III) transfer to form Mn(III)–T(4-CP)P occurs via ligand exchange, the rate of Mn(III)–T(4-CP)P formation from Mn(III) is slower than that of Mn(II). Experiments indicate the T(4-CP)P complexation rate of soluble Mn(III) is dependent on the strength of the original Mn(III) complex; i.e., the stronger the original Mn(III) complex, the slower the rate of T(4-CP)P complexation. Fig. 2 shows the ligand exchange kinetics of soluble Mn(III) complexes with different stability constants. The weaker of the two, Mn(III)-PP, has an estimated stability constant of $\log K = 16.7$ [21], while the Mn(III)-DFOB complex has a stability constant of $\log K = 29.9$ [7]. As a result, the rate of formation of Mn(III)–T(4-CP)P from Mn(III) complexes is very different. Greater than 95% complexation of the original Mn(III) takes place within approximately 5–15 min for Mn(III)-PP (1–10 μM), while more than 24 h are required for Mn(III)-DFOB (1–10 μM). Although there is significant difference in the complexation rate of various Mn(III) species with T(4-CP)P, as compared to the kinetics of Mn(II) complexation and subsequent oxidation, even the fastest complexation rate of known Mn(III) species is nearly an order of magnitude slower than that of Mn(II).

The rate of Mn(II) complexation and subsequent oxidation was determined to be independent of whether Mn(II) exists as a free ion or a complexed species. As shown in Fig. 2, the complexation and oxidation rate of Mn(II)-DFOB, a strong natural Mn(II) complex, is identical to the complexation and oxidation rate of Mn(II) as a free ion. Within the pH range of our experiments, total Mn(II) complexation for both species is complete in less than 1 min. Therefore, it is likely that the complexation and oxidation rate of natural Mn(II) species will have similar, if not identical rates.

Experiments also indicated that T(4-CP)P was unreactive towards colloidal MnO_2. As shown in Fig. 2, no Mn was removed and complexed by T(4-CP)P over the course of the experiment. Since colloidal MnO_2 is one of the most reactive forms of Mn oxide, Mn solid species found in natural waters should not cause interference.

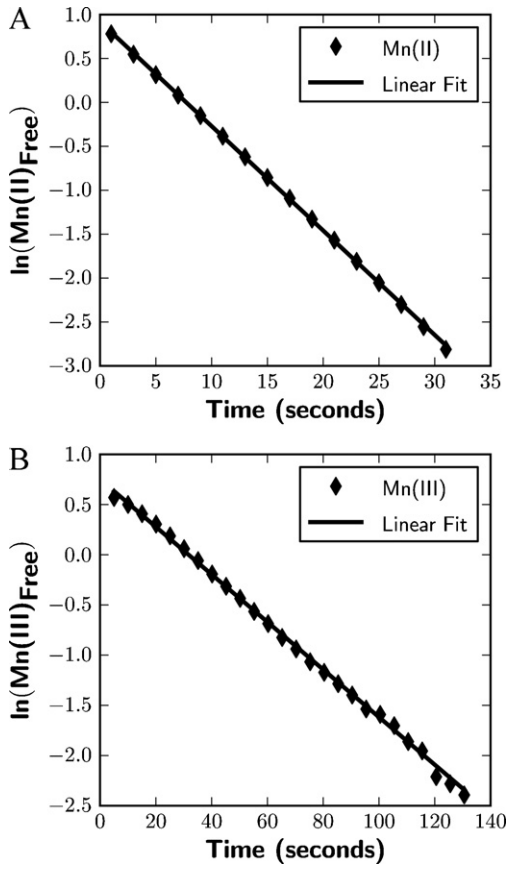

Fig. 3. ln[Mn] versus time plots show a pseudo first order behavior when T(4-CP)P was present in excess for both (A) Mn(II) and (B) Mn(III)-PP.

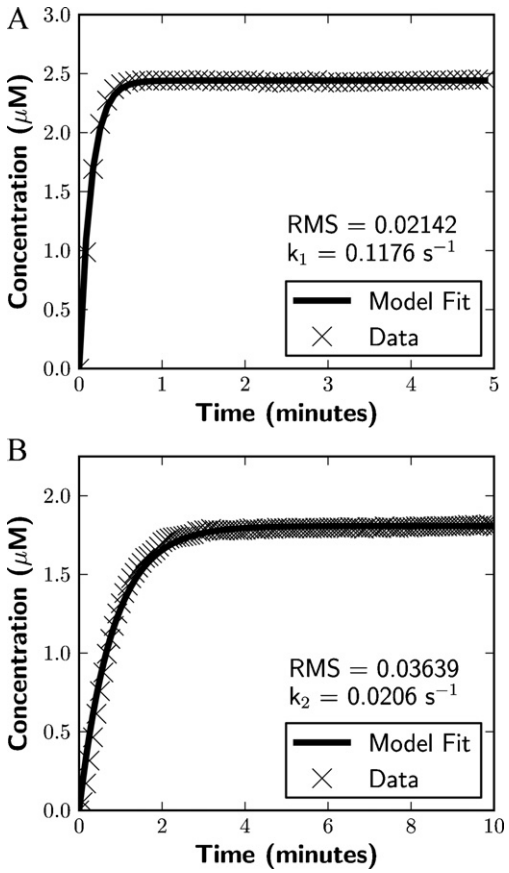

Fig. 4. Nonlinear least squares optimization of Eqs. (7) and (8) provide excellent fits for (A) Mn(II) and (B) Mn(III)-PP complexation with T(4-CP)P.

3.2. Rate law for Mn(II) and Mn(III) species

Ishii et al. [13] determined that once complexed by T(4-CP)P, Mn(II) is oxidized to form stable Mn(III)–T(4-CP)P. Therefore, assuming the time required for Mn(II) oxidation is short, in accordance with our experiments (Fig. 2), and T(4-CP)P is present in excess, the complexation of both Mn(II) and Mn(III) by T(4-CP)P can be approximated as pseudo-first order reactions. As seen in Fig. 3, plots of the logarithm of Mn concentration versus time confirm both Mn(II) and Mn(III) complexation reactions are first order. Therefore, the rates of Mn(III)–T(4-CP)P formation for both Mn(II) and Mn(III) complexes can be represented by:

$$\frac{d[\text{Mn(III)–T(4-CP)P}]}{dt} = -\frac{d[\text{Mn(II)}]}{dt} = k_1[\text{Mn(II)}] \tag{3}$$

$$\frac{d[\text{Mn(III)–T(4-CP)P}]}{dt} = -\frac{d[\text{Mn(III)}]}{dt} = k_2[\text{Mn(III)}] \tag{4}$$

Integrating Eqs. (3) and (4) for the respective Mn species with respect to time yields:

$$\text{Mn(II)} = \text{Mn(II)}_0 e^{-k_1 t} \tag{5}$$

$$\text{Mn(III)} = \text{Mn(III)}_0 e^{-k_2 t} \tag{6}$$

Since the concentration of the Mn species at a given time is equivalent to the difference of the original Mn concentration and Mn(III)–T(4-CP)P formed at the same time, the equations can be solved for Mn(III)–T(4-CP)P:

$$\text{Mn(III)–T(4-CP)P}_{\text{from Mn(II)}} = \text{Mn(II)}_0(1 - e^{-k_1 t}) \tag{7}$$

$$\text{Mn(III)–T(4-CP)P}_{\text{from Mn(III)}} = \text{Mn(III)}_0(1 - e^{-k_2 t}) \tag{8}$$

If a sample contains both Mn(II) and Mn(III) complexes, both species will contribute to the formation of Mn(III)–T(4-CP)P. Since T(4-CP)P is in large excess, the amount of T(4-CP)P removed by complexation with either Mn(II) or Mn(III) can be considered negligible. Therefore, total Mn concentration is simply equal to the sum of Eqs. (7) and (8):

$$[\text{Mn}]_{\text{Total}} = [\text{Mn(III)–T(4-CP)P}]_{\text{Total}} = \text{Mn(II)}_0(1 - e^{-k_1 t}) + \text{Mn(III)}_0(1 - e^{-k_2 t}) \tag{9}$$

3.3. Determination of Mn(II) and Mn(III)

To test the validity of Eqs. (5) and (6), known amounts of Mn(II) and Mn(III)-PP were added individually to T(4-CP)P solutions following the method described above. The resulting increase in absorbance of Mn(III)–T(4-CP)P was measured over time for each solution. A custom program written in the object-oriented programming language Python was used to fit Eqs. (5) and (6) to the respective Mn(III)–T(4-CP)P kinetic curves. The Mn(II) and Mn(III) concentrations and their respective complex formation rate constants, k_1, and, k_2, were determined using a nonlinear least squares minimization approach that optimized the values based on experimental kinetic data. Fig. 4 shows the results of the optimizations. Both Eqs. (5) and (6) provide excellent fits to the data with a root mean square error (RMSE) less than 0.04. Since the nonlinear portion of the curve is the most difficult to fit, the RMSE was also determined exclusively for the nonlinear region to prevent a bias in error reporting. In all experiments, this RMSE was always less than 0.07. Initial concentrations of Mn(II) and Mn(III) in laboratory-prepared solutions were accurately predicted within a range of 0.4–1% of the known values.

Table 1
Known amounts of Mn(II) and Mn(III)-PP were mixed in various concentrations. The T(4-CP)P kinetic method correctly determined the concentration within 0.4–2% of the known values.

Exp #	Added Mn(II) (μM)	Added Mn(III)-PP (μM)	Model Mn(II) (μM)	% Mn(II) Recovery	Model Mn(III) (μM)	% Mn(III) Recovery
1	2.50	0	2.51 ± 0.069	100.4	0	0
2	0	1.91	0	0	1.89 ± 0.050	99.0
3	2.40	1.90	2.41 ± 0.071	100.4	1.90 ± 0.034	100.0
4	5.00	1.90	5.08 ± 0.103	101.6	1.92 ± 0.065	101.1
5	2.40	3.78	2.39 ± 0.088	99.6	3.82 ± 0.149	99.0
6	5.00	3.81	5.10 ± 0.153	102.0	3.78 ± 0.095	99.2

The method also accurately determines the total Mn concentration in laboratory samples containing both dissolved Mn(II) and Mn(III) species. Several mixed Mn(II)/Mn(III)-PP samples containing various concentrations of each species were analyzed with the above procedure. The same custom Python program fit Eq. (9) to the Mn(III)–T(4-CP)P kinetic data. The variables optimized were: $[Mn_0^{II}]$, $[Mn_0^{III}]$, k_1 and k_2. The result of a nonlinear least square optimization is shown in Fig. 5. For all experiments, excellent fits were obtained with a root mean square error of less than 0.03. For each experiment listed in Table 1, triplicate kinetic runs were performed and initial concentrations of Mn(II) and Mn(III) were predicted within 0.4–2% of the known Mn(II) and Mn(III) concentrations, for all 18 experiments.

The only source of error in the procedure is due to the photodecomposition of Cd(II)–T(4-CP)P in the cell, which is easily corrected. Experimentation determined ≤1% of Cd(II)–T(4-CP)P photodecomposes during a 15 min kinetic run when light from the UV/vis source passes through the sample solution. During photodecomposition, the Cd(II)–T(4-CP)P peak broadens at its base and overlaps with the Mn(III)–T(4-CP)P peak, which contributes slightly to the absorbance of Mn(III)–T(4-CP)P. Without correction, the absorbance of Mn(III)–T(4-CP)P does not level off and there is always a slight increase in absorbance through time. The problem is easily corrected by measuring the increase in absorbance at 468 nm of several reagent blank samples over the 15 min time period at the same 5 s sampling intervals. The absorbance at each time is then subtracted from the kinetic curve of the Mn sample. This correction yields smooth exponential absorbance curves that rise to a steady maximum. This correction was applied to all samples analyzed in the laboratory and in the field.

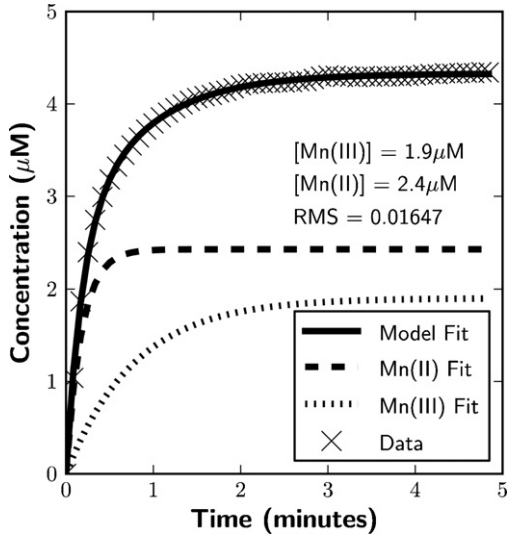

Fig. 5. Nonlinear least squares optimization of a mixed Mn(II)/Mn(III) laboratory sample accurately predicts Mn(II) and Mn(III) concentration to within 0.4–2% of their known values.

3.4. Mn(II) and Mn(III) detection limits

The detection limit for the two soluble Mn oxidation states [Mn(II) and/or Mn(III)] can be defined despite its dependency on the quality of the model fit and the chemistry of the sample matrix. Determination of Mn(II) and Mn(III) requires a sufficient increase in Mn(III)–T(4-CP)P absorbance over time for accurate optimization. Experimentation at low Mn(II) and Mn(III) levels revealed that the linear least squares optimization requires an absorbance increase of approximately 0.01 absorbance units with a 5 s sampling frequency. For this reason, the kinetic method's estimated detection limit is currently 100 nM for a 1 cm pathlength cell, approximately twice the detection limit for total soluble Mn defined by Ishii et al. [13] and this work. The linear least squares method was used for its simplicity and accuracy; however a more complicated and accurate optimization method might offer a lower detection limit when both Mn(II) and Mn(III) are present.

A further complication in determining the method's detection limit, which was first investigated by Ishii et al. [13], is that high concentrations of chloride interfere with the measurement. Specifically, Cd-chloro complexes form rapidly, which remove Cd from T(4-CP)P and slow the metal exchange of Cd with Mn. While this is not a problem in freshwater environments, it can interfere with analyses in saline environments, such as coastal and ocean waters and sediment porewaters. Therefore, accurate analysis of coastal and/or marine sediment porewaters requires a dilution of the sample with deionized water to lower the chloride ion concentration (<0.2 M) and limit its interference. To date, the method has been used for aqueous samples ranging from low (fresh/salt marsh) to open ocean salinities (5–35 ppt) and experiments determined a 1/3 dilution of marine sediment porewaters is enough to prevent chloride interference. In the procedure, ≤1 mL of a high salinity sample is diluted in the spectrophotometric cell following the addition of ≥2 mL mix of reagents and deionized water. The Mn species detection limit of a freshwater sample, free of chloride, is 100 nM because no dilution is necessary, but for a saltwater sample, accounting for the 1/3 dilution, the detection limit is 300 nM. Although dilution is necessary in certain environments, this is still a significant improvement over the formaldoxime method, which is inaccurate at Mn concentrations lower than 1 μM [14].

3.5. Possible interferences

The Soret band of the Mn(III)–T(4-CP)P complex is a sensitive peak that is not prone to interference by neighboring peaks. Ishii et al. [13] and this work determined that most cations and anions do not interfere with accurate determination of Mn. Mn ligands present in laboratory solutions and natural samples do not interfere with Mn determination because T(4-CP)P is present in large excess. To date, all natural Mn(III) complexes have been completely outcomplexed by T(4-CP)P within 15-min.

3.6. Qualitative estimate of natural Mn(III) complexes

As discussed earlier, the complex formation rates k_1 and k_2 were determined for Mn(II) and Mn(III) upon least squares optimization. While k_1 remains the same for Mn(II) in all experiments, k_2 depends on the Mn(III) complex(es) present, due to competition between the Mn(III) ligand(s) and T(4-CP)P. In this study, the revised T(4-CP)P procedure was tested on two known Mn(III) complexes, both of which have different stabilities, reactivities and k_2 values. Currently, little is known of the reactivity of natural Mn(III) complexes. A comparison with known Mn(III) complexes, such as Mn(III)-PP and Mn(III)-DFOB used in this study, would offer a semi-quantitative estimate of the reactivity (via the k_2 value) of naturally occurring Mn(III) complexes. A general estimate is valuable in understanding the reactivity and possible stability of natural Mn(III) species.

3.7. Determination of soluble Mn(II) and Mn(III) in sediment porewaters of the Lower St. Lawrence Estuary

The kinetic method was used during a July 2009 research cruise in the Lower St. Lawrence Estuary (Quebec, Canada) to determine soluble Mn(II) and Mn(III) concentrations in sediment porewaters. The Lower St. Lawrence Estuary is an ideal location to develop and validate methods for Mn determination because it is a hemipelagic system with Mn-rich sediments [22]. Total soluble Mn porewater concentrations are greater than 100 μM at many sites within the estuary [23].

The new procedure successfully determined Mn(II) and Mn(III) porewater concentrations recovered from a 40 cm long sediment core. A typical kinetic curve from a porewater sample extracted from the 1–2 cm depth interval is shown in Fig. 6. Analogous to the mixed Mn(II)/Mn(III) laboratory solutions, the model provides an excellent fit to the curve and, therefore, accurate Mn(II) and Mn(III) concentrations, with little experimental/model error.

The Mn porewater profile at Station 23 is shown in Fig. 7A. As seen in Fig. 7, the most intense Mn cycling zone occurs within the upper 5 cm of the sediment column. In this region, Mn(III) complexes account for 10–84% of the dissolved Mn pool (Fig. 7B). These Mn(III) complexes are most likely formed as dissolved Mn(II) from the deeper, anoxic sediments diffuses upwards into the suboxic layer where Mn oxidizing microbes use trace O_2 to oxidize Mn(II) to Mn(III) [24,25]. Mn(III) may also be generated during the reduction of Mn(IV) oxides by Fe(II) and H_2S (unpublished work not shown). Fig. 7 demonstrates that once formed, Mn(III) complexes are mainly found in the upper suboxic and oxic sediments (depth of O_2 penetration was near 1 cm as determined by microelectrode work; data not shown). The Mn porewater profile indicates that the upward and downward Mn(III) concentration gradients drive fluxes both upwards (and possibly out of the sediment) and downwards where the Mn(III) complexes can participate as electron acceptors in biogeochemical cycles. A comparison of the optimized k_2 values (indicative of reactivity) at each depth interval suggests that the natural Mn(III) complexes are less reactive than Mn(III)-PP, but more reactive than Mn(III)-DFOB.

As the sediments become more reducing with depth, Mn(III) complexes are reduced to Mn(II), until their presence becomes undetectable.

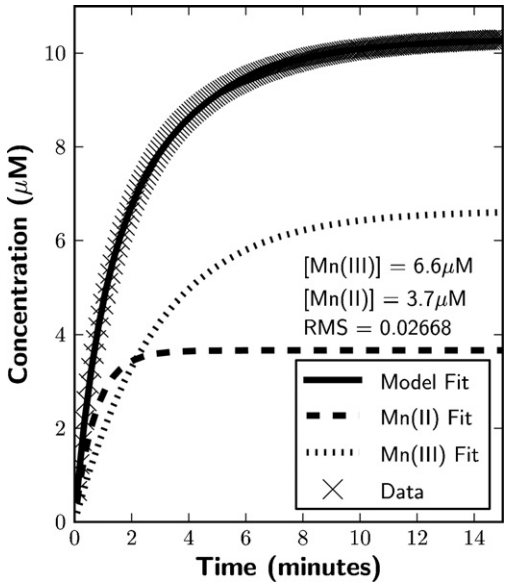

Fig. 6. Example T(4-CP)P kinetic curve obtained from the analysis of a porewater sample extracted from the 1–2 cm depth interval collected at Station 23 in July, 2009.

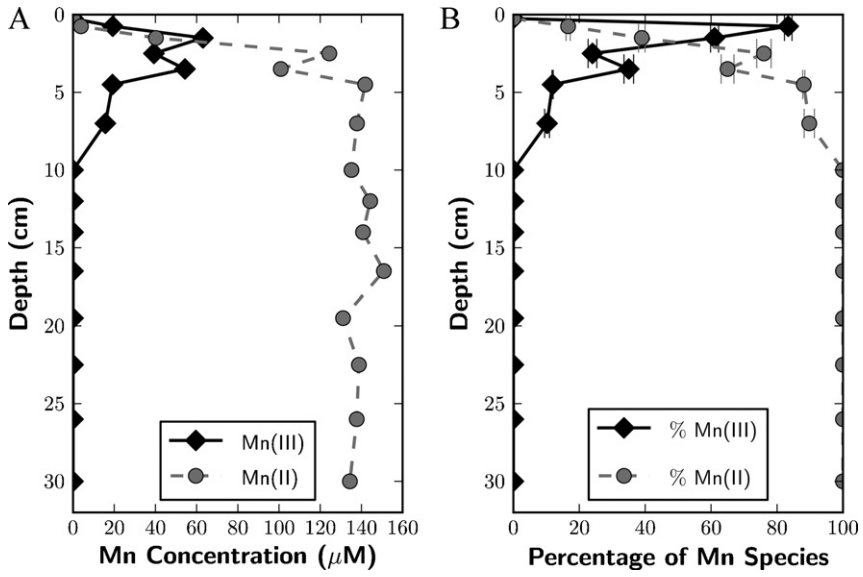

Fig. 7. (A) Mn porewater profile collected at Station 23 in the Lower St. Lawrence Estuary during a research cruise in July, 2009. (B) The percentage of the total soluble Mn pool for dissolved Mn(II) and Mn(III) was also determined.

Table 2
Method comparisons show agreement between results T(4-CP)P and ICP-MS analyses, while both disagree with results of the formaldoxime method.

Depth (cm)	T(4-CP)P $\sum$Mn (μM)	T(4-CP)P error (μM)	ICP-MS $\sum$Mn (μM)	ICP-MS error (μM)	Formaldoxime $\sum$Mn (μM)
1.5	103.3	0.81	103.9	2.26	85.0
7	153.6	2.30	153.3	3.79	140.9
16.5	150.9	0.16	150.4	3.48	133.1

3.8. Mn method comparisons

A comparison with three other Mn methods was performed on the field samples. First, the formaldoxime method [18] was used to determine total soluble Mn. As discovered by Chiswell and O'Halloran [14], the concentration of soluble Mn determined with the formaldoxime method often did not agree with results of the T(4-CP)P method. As shown in Fig. 8, the methods are most inconsistent in the upper layers of the sediment, where soluble Mn(III) complexes occur. It is likely that formaldoxime is unable to reduce and complex Mn(III) bound to strong natural ligands. Deeper in the sediment, total soluble Mn concentrations determined via the formaldoxime method are consistent with the results of the T(4-CP)P method, most likely because Mn(III) is absent.

Second, for select depth intervals, inductively coupled plasma mass spectrometry (ICP-MS) was used to quantify total soluble Mn in the porewaters. As shown in Table 2, the results of the porphyrin and ICP-MS methods agree within 0.4%, but both are more than 10% larger than those obtained on the same samples by the formaldoxime method. Since the formaldoxime method values do not exhibit any overall trends, suggestive of systematic experimental error, the data comparisons indicate the formaldoxime method is inaccurate for measurement of total soluble Mn in this sedimentary environment. The T(4-CP)P method is not only a significant improvement in terms of sensitivity and accuracy over the formaldoxime method for the determination of total soluble Mn, but provides a means to discriminate between Mn(II) and Mn(III) oxidation states simultaneously.

A third method taken from Trouwborst et al. [10] (which uses DFOB to out-complex Mn(III) in natural Mn(III) complexes, followed by voltammetric measurement as Mn(III)-DFOB) was used to determine soluble Mn(III) in the sediment porewaters. Although this method was not optimized for porewater analysis (the voltammetric method is more labor intensive and not as sensitive as the T(4-CP)P method because of sample dilution into a buffer), results were within a 95% confidence interval of the concentration of soluble Mn(III) determined by the new T(4-CP)P method.

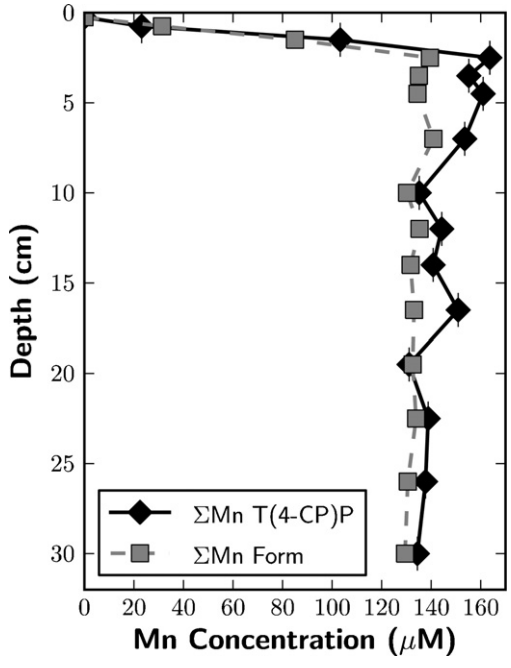

Fig. 8. Comparison of total soluble Mn concentrations determined by the recommended T(4-CP)P procedure and the formaldoxime method.

3.9. Potential application to other environments

The T(4-CP)P kinetic method, thus far, has been applied to porewater samples extracted from a hemipelagic system and salt marsh sediments, but is applicable to a variety of environments where Mn concentration is greater than 50–100 nM. Potential environments for which the T(4-CP)P kinetic method is useful include groundwater, lakes and rivers, freshwater marshes and larger bodies of water (e.g., the Black Sea and the Chesapeake Bay) where Mn concentrations are greater than 50 nM.

4. Conclusions

A reliable and relatively quick (20 min per sample) analytical method for the simultaneous determination of soluble Mn(II) and Mn(III) in natural (pore)waters was developed. The kinetic procedure yields results that agree well with those obtained from a standard total soluble Mn method (ICP-MS) and a direct method for the determination of Mn(III) [10]. The method accurately determined Mn(II) and Mn(III) concentrations simultaneously in laboratory solutions and sediment porewater samples recovered from the Lower St. Lawrence Estuary. The kinetic T(4-CP)P method meets the following requirements: (1) the method simultaneously determines soluble Mn(II), Mn(III) and total Mn, (2) soluble Mn(II), Mn(III) and total Mn determination is accurate, (3) the analysis employs simple instrumentation and (4) the estimated detection limit for both Mn(II) and Mn(III) is 100 nM with small sample volumes. In addition to accurately determining Mn(II) and Mn(III) concentrations, a comparison of the T(4-CP)P complexation rate constant (k_2) of natural and known (e.g., Mn(III)-PP and Mn(III)-DFOB) Mn(III) complexes provides an estimate of the relative stability/reactivity of the former. The new T(4-CP)P method was optimized for natural water samples and is one of two direct methods capable of providing critical information on Mn cycling and natural Mn(III) complexes in natural waters.

4.1. Code availability

The Python source code used to determine soluble Mn(II) and Mn(III) is available for use/modification as an online supplement to this article.

Acknowledgements

We are grateful to the Natural Sciences and Engineering Research Council of Canada (NSERC) for financial support of the shiptime on the R/V Coriolis through a grant to Bjorn Sundby and Alfonso Mucci. We thank Bjorn Sundby and Alfonso Mucci for their invitation to participate in the research cruise and their helpful comments during preparation of the manuscript. We are grateful to the crew of the R/V Coriolis for their hard work and thoughtfulness

throughout the research cruise. We thank Amy Gartman, who analyzed the porewater samples via ICP-MS. This work was supported by grants from the U.S. National Oceanic and Atmospheric Administration Sea Grant program (NA09OAR4170070) and from the U.S. National Science Foundation (OCE-1031272 and OCE-1031200).

Appendix A. Supplementary data

Supplementary data associated with this article can be found, in the online version, at doi:10.1016/j.talanta.2011.01.025.

References

[1] J.K. Klewicki, J.J. Morgan, Environ. Sci. Technol. 32 (1998) 2916–2922.
[2] A. Schippers, L.N. Neretin, G. Lavik, T. Leipe, F. Pollehne, Geochim. Cosmochim. Acta 69 (2005) 2241–2252.
[3] L.N. Neretin, C. Pohl, G. Jost, T. Leipe, F. Pollehne, Mar. Chem. 82 (2003) 125–143.
[4] L.S. Balistrieri, J.W. Murray, Geochim. Cosmochim. Acta 46 (1982) 1041–1052.
[5] B.M. Tebo, Deep Sea Res. A 38 (1991) S883–S905.
[6] S. Emerson, S. Kalhorn, L. Jacobs, B. Tebo, K. Nealson, R. Rosson, Geochim. Cosmochim. Acta 46 (1982) 1073–1079.
[7] O.W. Duckworth, G. Sposito, Environ. Sci. Technol. 39 (2005) 6037–6044.
[8] J.E. Kostka, G.W. Luther, K.H. Nealson, Geochim. Cosmochim. Acta 59 (1995) 885–894.
[9] D.L. Parker, G. Sposito, B.M. Tebo, Geochim. Cosmochim. Acta 68 (2004) 4809–4820.
[10] R.E. Trouwborst, B.G. Clement, B.M. Tebo, B.T. Glazer, G.W. Luther, Science 313 (2006) 1955–1957.
[11] E.V. Yakushev, F. Pollehne, G. Jost, I. Kuznetso, B. Schneider, L. Urnlauf, Mar. Chem. 107 (2007) 388–410.
[12] E. Yakushev, S. Pakhomova, K. Sorenson, J. Skei, Mar. Chem. 117 (2009) 59–70.
[13] H. Ishii, H. Koh, K. Satoh, Anal. Chim. Acta 136 (1982) 347–352.
[14] B. Chiswell, K.R. O'Halloran, Talanta 38 (1991) 641–647.
[15] J.F. Perez-Benito, E. Brillas, R. Pouplana, Inorg. Chem. 28 (1989) 390–392.
[16] A. Mucci, B. Boudreau, C. Guignard, Appl. Geochem. 18 (2003) 1011–1026.
[17] W.S. Reeburgh, Limnol. Oceanogr. 12 (1967) 163–165.
[18] P.G. Brewer, D.W. Spencer, Limnol. Oceanogr. 16 (1971) 107.
[19] D.C. Harris, Quantitative Chemical Analysis, 6th ed., W.H. Freeman and Company, New York, 2003.
[20] D. Lieb, A. Zahl, T.E. Shubina, I. Ivanovicĭ-Burmazovicĭ, J. Am. Chem. Soc. 132 (2010) 7282–7284.
[21] V. Gordienk, V. Sidorenk, Y. Mikhaily, Zh. Neorg. Khim. 15 (1970) 2379.
[22] P. Anschutz, B. Sundby, L. Lefrancois, G.W. Luther, A. Mucci, Geochim. Cosmochim. Acta 64 (2000) 2751–2763.
[23] S. Katsev, G. Chaillou, B. Sundby, A. Mucci, Limnol. Oceanogr. 52 (2007) 2555–2568.
[24] B.M. Tebo, J.R. Bargar, B.G. Clement, G.J. Dick, K.J. Murray, D. Parker, R. Verity, S.M. Webb, Annu. Rev. Earth Planet Sci. 32 (2004) 287–328.
[25] B. Clement, G. Luther, B. Tebo, Geochim. Cosmochim. Acta 73 (2009) 1878–1889.